Second Conference on Smart Monitoring,
Assessment and Rehabilitation of Civil Structures

SMAR 2013

Pultruded GFRP Square Hollow Sections (SHS) under Transverse Bearing Load

Chao Wu and Yu Bai*

Department of Civil Engineering, Monash University, Melbourne, VIC 3800, Australia

ABSTRACT: This paper presents an experimental study on the web crippling behaviour of GFRP square hollow sections (SHS) subjected to concentrated transverse bearing load. Four pultruded GFRP SHS were adopted with various web slenderness ratios. Each section was tested under end-two-flange (ETF) and interior-two-flange (ITF) loading conditions. Another two loading conditions were also considered where tested specimens sit on the flat ground with end (G-ETF) or interior (G-ITF) concentrated loading applied through a rigid bearing plate. Different failure modes were observed including web-flange junction failure, web shear/bending failure and web crushing failure. An interesting two-stage failure process was noticed for all specimens from the corresponding load-displacement curves. "Elastic limit" load and ultimate failure load were thus defined. The effects of web slenderness ratio and four loading conditions on the web crippling behaviour were discussed. This study overall provides a basis for further work into the growing field of FRP composites in construction.

1 INTRODUCTION

Pultruded glass fiber reinforced polymer (GFRP) composites have gained wide applications in civil infrastructure (Keller 2003), due to the advantages of lightweight, ease of installation, low maintenance, and resistance to harsh environmental conditions (Hollaway 1993 and 2009). Tubular GFRP sections perform well in the pultruded direction according to the manufacturing process. However, web crippling failure becomes critical when transverse concentrated loading is applied, i.e. support reaction force, or transverse bearing load from other structural members.

Extensive experimental research has been conducted on web crippling strength of tubular metallic sections (Packer 1984, Zhao and Hancock 1992, Zhou and Young 2007 and 2008). Four loading conditions have been adopted according to existing design rules (NAS 2001 and AS/NZS 4673 2001), namely end-one-flange (EOF), interior-one-flange (IOF), end-two-flange (ETF) and interior-two-flange (ITF). The loading conditions are classified based on the concentrated load acting on one flange only or both flanges as well as the location of the applied load (Zhou and Young 2008). Zhao and Hancock (1995), Young and Hancock (2003) conducted a series of tests on cold-formed steel sections subjected to concentrated bearing load, where the specimens were seated on a fixed solid steel base plate. In this way, the support condition of the floor joist members seated on solid foundations was closely represented.

To date there has been limited research conducted on pultruded tubular GFRP profiles subjected to web crippling under concentrated loading. Web buckling strength of multi-cellular FRP bridge deck module was experimentally investigated by Prachasaree and GangaRao (2009). FRP bridge deck of 76.2×73.7 cm were put on a flat solid foundation. Truck loading

was simulated by applying compression over the top flange of FRP bridge deck modules, through a thick plate with a dimension of 25.4×50.8 cm. It was found that crack initiated at web-flange junction and propagated along the longitudinal direction of the web. In terms of web-buckling strength, single web specimens performed better than specimens with multi-webs. This was attributed to the bending stress at the web-flange junction introduced by the compression load. Borowicz and Bank (2010) investigated the behaviour of pultruded GFRP beams subjected to concentrated loads in the plane of the web. 20 pultruded GFRP I beams with nominal depths from 152.4 to 304.8 mm were tested in three-point bending with a span-to-depth ratio of 4. Concentrated loading was applied to the top flange directly: 12 beams without bearing plates and 8 beams with bearing plates. Global stability failure was avoided through lateral supports. All specimens failed with a wedgelike shear failure at the upper web-flange junction. The experimental results showed that the introduction of bearing plates increased the ultimate capacity of the beams by at least 35%. However, only IOF loading was anglicised in previous studies and more loading conditions need to be investigated.

This paper presents experimental program on tubular pultruded GFRP profiles subjected to web crippling under concentrated loading. Four GFRP square hollow sections (SHS) of various sectional dimensions are selected to study the effect of web slenderness ratio. Both ETF and ITF loading conditions are adopted, with concentrated loading applied simultaneously and symmetrically on top and bottom flanges of GFRP sections. Specimens are also put on solid foundation with applied end or interior concentrated loading to simulate the support condition of the floor joist members. Transverse bearing load was applied through a rigid bearing plate of 50 mm width. Failure modes were recorded by a video camera. A two-stage failure process was observed from load-displacement curves. Then an “elastic limit” load and an ultimate failure load were defined accordingly. The results can serve as experimental data base for future development of web crippling design rules for pultruded GFRP sections.

2 EXPERIMENTAL PROGRAM

2.1 Tubular pultruded GFRP SHS sections

In the present study, four tubular pultruded GFRP SHS sections were chosen for the experimental program. The nominal sectional dimensions are presented in Table 1. The section ID is given by the initial “S” referring to the square section. The manufacturer provided nominal material properties are presented in Table 2.

Table 1. Tubular pultruded GFRP SHS sections

Section ID.	Total height H (mm)	Wall thickness t (mm)	Web slenderness ratio (H-2t)/t
S1	102	5.3	17.2
S2	102	10	8.2
S3	50	4	10.5
S4	50	6	6.3

Table 2. Nominal material properties of GFRP sections

Measurement direction	Properties	Unit	Values
Pultruding	Tension modulus	GPa	23
	Tension strength	MPa	240
Transverse	Tension modulus	GPa	7
	Tension strength	MPa	50
Interlaminar	Shear strength	MPa	25

2.2 Experiment set-up and instrumentation

All tests were performed on a Baldwin Universal testing machine. Two loading conditions, end-two-flange (ETF) and interior-two-flange (ITF), were adopted for all the GFRP sections. Furthermore, in order to represent the loading condition of floor joist members, end bearing load and interior bearing load were also applied on "S2", "S3"and "S4" sections by putting them on the fixed rigid steel base. The four loading conditions are illustrated in Figure 1. The length of each section varies depending on the adopted loading condition, as listed in Table 3. The length of each specimen is much longer than the required length, i.e. 1.5 times of the total height of the web as specified in NAS (2001) and the AS/NZS 4100 (1998) for cold-formed steel structures.

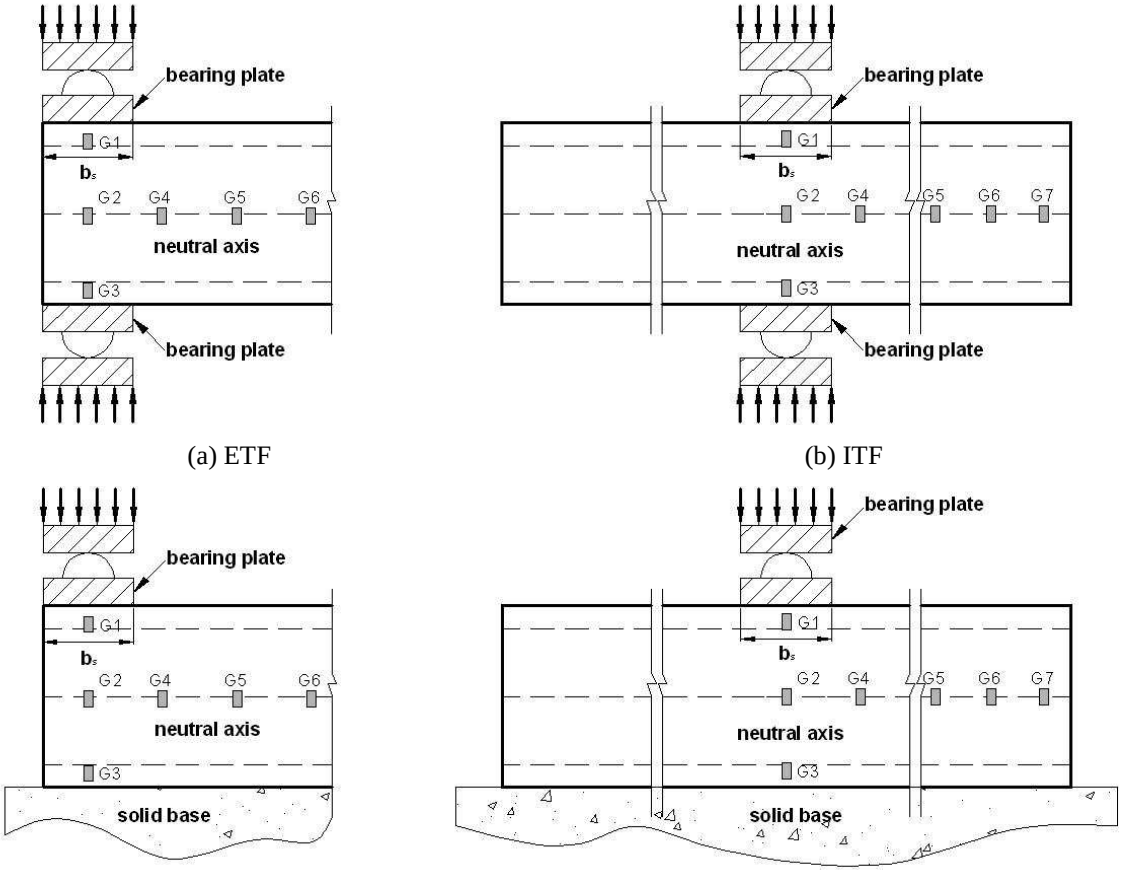

(a) ETF (b) ITF

(c) G-ETF (d) G-ITF

Figure 1. Illustration of loading conditions: (a) and (b) are applied to all sections; (c) and (d) are applied to "S2", "S3" and "S4" sections

The load was applied through a rigid bearing steel plate of 50 mm width, b_s in Figure 1. The bearing plate was big enough to act across the full flange widths of all GFRP sections. The flanges of the GFRP sections were neither fastened (unrestrained) to the bearing plates, nor to the solid steel base during the testing. The compressive loading was applied in displacement control at a loading speed of 0.5 mm/min for all the specimens.

Table 3. Selected specimen length and strain gauge spacing

Section ID.	Specimen length (mm)		Strain gauge spacing (mm)	
	ETF and G-ETF	ITF and G-ITF	ETF and G-ETF	ITF and G-ITF
S1 and S2	300	600	65	70
S3 and S4	200	400	40	45

Seven strain gauges, G1~G7 in Figure 1, were attached on the web of each specimen for identifying the specimen length affected by the concentrated loading. The spacing of strain gauges G1~G3 is equal to the half depth of the corresponding section (H/2), and the spacing of strain gauges G4~G7 is listed in Table 3. A video camera was used for recording the progressive failure of all the specimens. The experimental setup is shown in Figure 2.

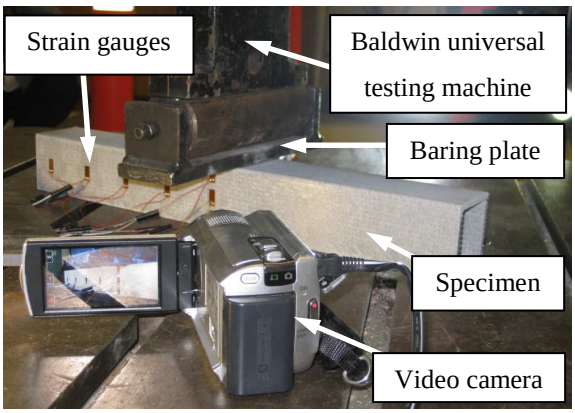

Figure 2. Experimental setup and instrumentations

3 EXPERIMENTAL RESULTS AND DISCUSSION

All the tested GFRP SHS specimens are listed in Table 4. The label of each specimen is comprised of three parts. The first part is the GFRP section ID as given in Table 1. The second part is the loading condition, as illustrated in Figure 1. In the following discussions of the paper, the terms, i.e. ETF, ITF, G-ETF, G-ITF, will be used to describe the four loading conditions. The number, "-1" or "-2" refers to the repeat tests.

3.1 Failure modes

Several failure modes were detected during the loading process of GFRP sections, as depicted in Figure 3. For specimens under ETF (Figure 3a) and ITF (Figure 3b) conditions, the shear crack initiated at the web-flange junction before the webs were crushed in shear or bending depending on the web slenderness ratio. Similar shear crack initiation was observed at top web-flange junctions of specimens sitting on the ground (G-ETF or G-ITF), as shown in Figure 3c and 3d. The difference is the lower portion of the GFRP section kept intact. This is probably because that the concentrated bearing force on the top flange can be effectively spread to a larger supporting area.

Table 4. Elastic limit load and ultimate load for all tested specimens

Specimens	Elastic limit load	Ultimate load
	P_e (kN)	P_{max} (kN)
S1-ETF-1	10.6	14.2
S1-ETF-2	15.1	15.4
S1-ITF-1	26.9	30.3
S1-ITF-2	26.6	29.9
S2-ETF-1	19.7	26.2
S2-ETF-2	26.1	26.8
S2-ITF-1	42.8	45.3
S2-ITF-2	40.1	48.5
S3-ETF-1	12.2	15.5
S3-ETF-2	12.9	13.9
S3-ITF-1	16.4	21.2
S3-ITF-2	15.8	19.4
S4-ETF-1	13.6	15.1
S4-ETF-2	22.7	25.5
S4-ETF-3	18.7	21.9
S4-ITF-1	20.4	32.0
S4-ITF-2	27.3	28.8
S2-G-ETF-1	20.8	32.4
S2-G-ETF-2	18.8	33.2
S2-G-ITF-1	48.6	52.3
S2-G-ITF-2	47.6	50.5
S3-G-ETF-1	11.0	14.4
S3-G-ETF-2	11.7	15.4
S3-G-ETF-3	11.4	16.4
S3-G-ITF-1	12.5	22.3
S3-G-ITF-2	15.8	23.4
S4-G-ETF-1	14.6	21.7
S4-G-ETF-2	16.4	21.0
S4-G-ETF-3	20.0	21.5
S4-G-ITF-1	29.5	31.8
S4-G-ITF-2	24.8	29.0

3.2 Strain distribution

Seven strain gauges were attached on the web of each section to record the strain distribution through loading process (Figure 4a). In this way, the "effective length" of GFRP section for carrying the concentrated bearing load can be measured. The "effective length", L_e in Figure 4a, is defined as the length beyond which the transverse strain on the neutral axis of the web becomes zero at the ultimate bearing load "P_{max}". Figure 4(b) presents "effective length" of four GFRP sections (average value of repeated tests was adopted here). It can be seen that the effective lengths of all GFRP sections are well within the selected specimen lengths as given in Table 3 and sections S1 and S2 presented much longer effective length than the other two because of they are taller in height and thus the bearing load can be sustained by longer web.

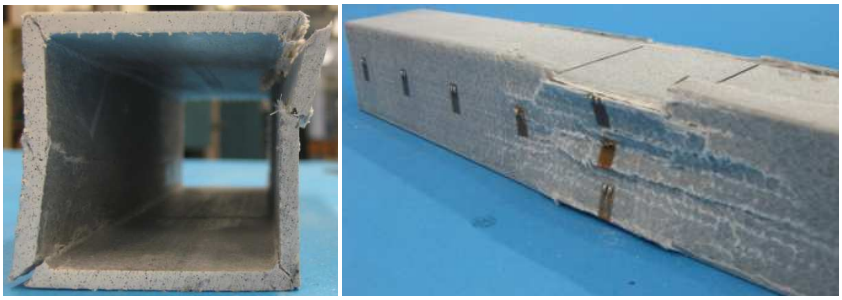

(a) ETF (b) ITF

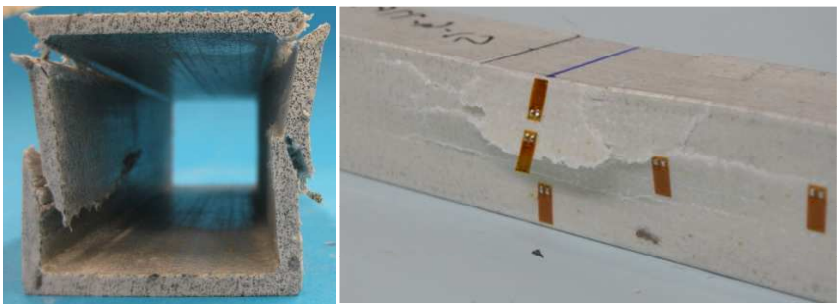

(c) G-ETF (d) G-ITF

Figure 3. Typical failure modes of GFRP sections under various loading conditions.

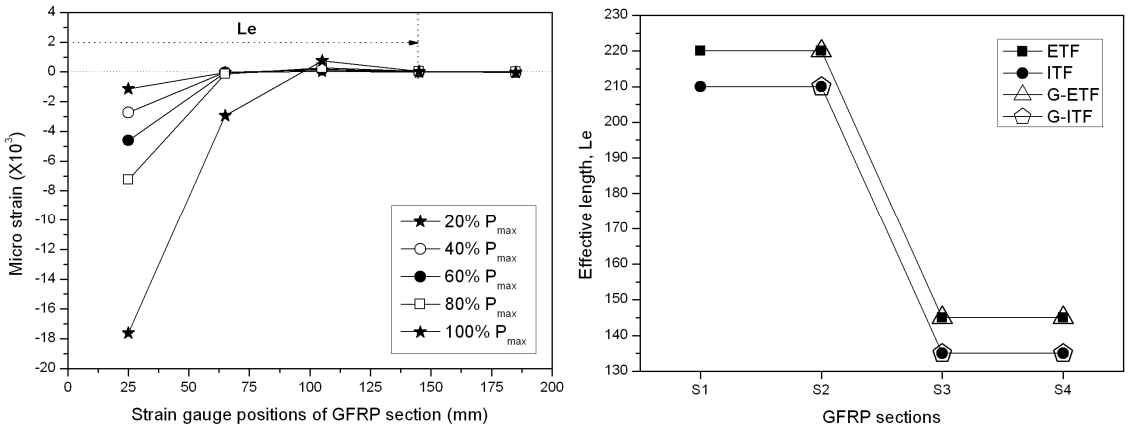

(a) (b)

Figure 4. (a) Typical strain distribution with load (S2-ETF-2); (b) Effective lengths of all GFRP sections.

3.3 Load-displacement curves and web crippling strength

The load-displacement curves of all GFRP sections under various loading conditions are plotted in Figure 5. It can be seen that the load drops at the end of the linear load-displacement branch, before the ultimate load is reached. The "elastic limit" load is defined as the first peak load which occurred at the end of the linear branch of the load-displacement curve of corresponding test. Secondly, comparing to (G-)ETF, (G-)ITF specimens exhibit much higher "web crippling capacity" (maximum load in the load-displacement curves). This is straightforward because the

interior bearing load can be transferred and sustained by larger web areas in the longitudinal direction. Finally, it seems specimens on the ground obtain higher, although not considerable, "web crippling capacities" than those placed on top of bearing plate. As mentioned before, the solid ground tends to spread the bearing load to a larger supported area.

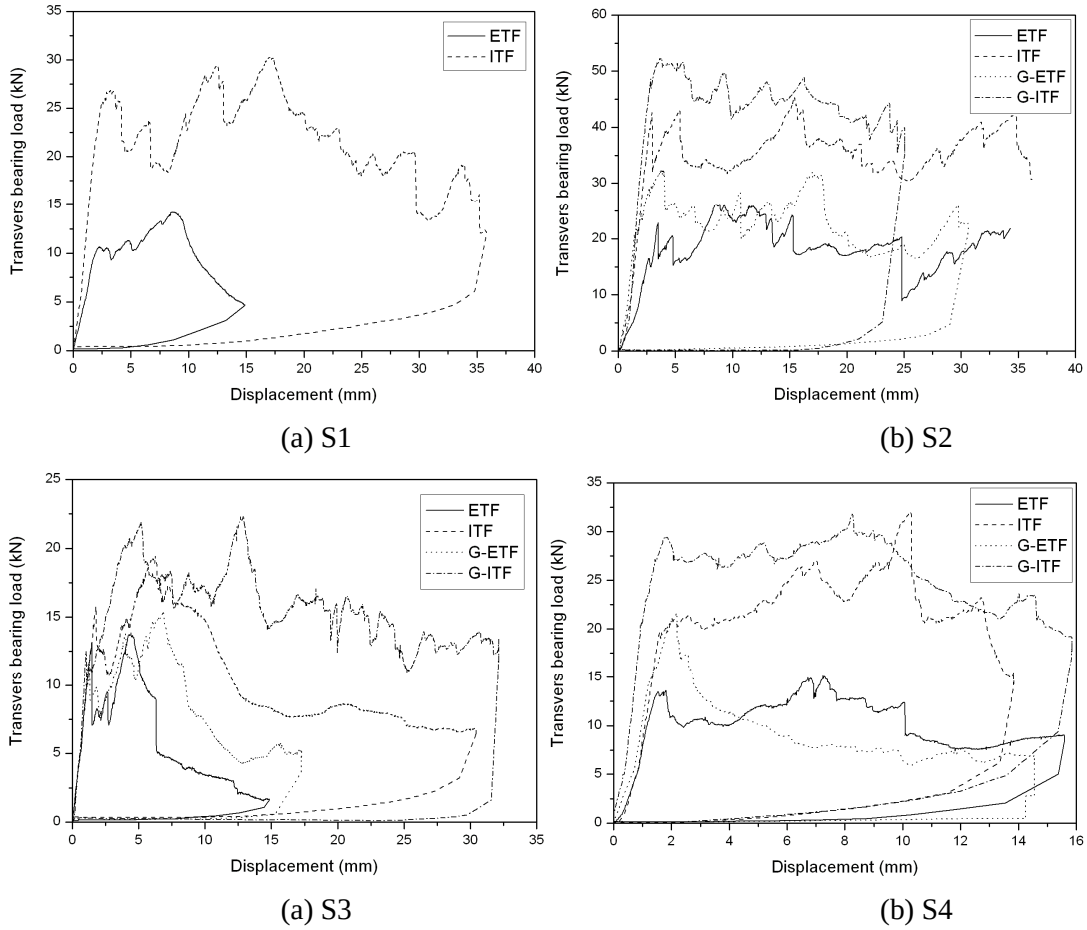

Figure 5. Load displacement curves of all GFRP sections under various loading conditions.

4 CONCLUSIONS

This paper presents an experimental study on the web crippling behaviour of pultruded GFRP sections. Four tubular GFRP SHS sections were tested under four loading conditions of ETF, ITF, G-ETF and G-ITF. Strain gauges were attached on the web to illustrate the load transfer mechanism. Progressive failure was recorded by video camera and different failure modes were observed. According to the experimental results, the following conclusions can be made:

- Under transverse (end or interior) bearing load, the failure initiated at the web-flange junction of GFRP section. With the bearing load increased, web shear or bending failure occurred. It was also found that the lower portion of GFRP section kept intact when the specimen sit on the ground.
- A two-stage failure process was found for all GFRP sections. The first stage was linear elastic which terminated at an "elastic limit" load. The second stage was featured by the

load fluctuation with the displacement. “Web crippling strength” was defined by the peak point of load-displacement curve.

- It was indicated that, comparing to end bearing load, specimens exhibited higher web crippling strengthen when interior bearing load was applied. Also, when specimens sitting on the ground, the web crippling strength can also be increased comparing to specimens sitting on bearing plate.

Theoretical analysis to predict web crippling strength of tubular GFRP sections is currently conducted by the authors and such results are expected for designing tubular GFRP sections in structural construction.

5 ACKNOWLEDGEMENT

The authors gratefully acknowledge the financial support provided by the Australian Research Council through a Discovery Early Career Researcher Award and the Travel Grant provided by CASS Foundation to attend the conference. The authors also wish to thank Mr. Xiang Ji, Mr. Patric Morgan and Mr. Kevin Nievaart for their assistance in carrying out the experimental testing in Civil Engineering Laboratory in Monash University.

6 REFERENCES

AS/NZS 4100: 1998. *Steel structures*. Australian/New Zealand Standard, Sydney (Australia): Standards Australia.

Borowicz, DT and Bank, LC. 2010. Behavior of pultruded fiber-reinforced polymer beams subjected to concentrated loads in the plane of the web. *Journal of Composites for Construction*, 15(2): 229-238.

Hollaway, LC. 1993. Polymer composites for civil and structural engineering. London: Chapman & Hall.

Hollaway, LC. 2009. Polymer composites in construction: a brief history. *Proceedings of the ICE - Engineering and Computational Mechanics*, 162(3): 107-118.

Keller, T. 2003. *Use of fiber reinforced polymers in bridge construction*. Structural Engineering Documents, No. 7, International Association for Bridge and Structural Engineering IABSE, ISBN 3-85748-108-0.

NAS. 2001. *North American specification for the design of cold-formed steel structural members*, American Iron and Steel Institute, Washington, DC.

Packer, JA. 1984. Web Crippling of Rectangular Hollow Sections. *Journal of Structural Engineering*, 110(10): 2357-2373.

Prachasaree, W and GangaRao, HVS. 2009. Web buckling strength evaluation of multicellular frp bridge deck module, *ICET-2009-4th International Conference on Engineering Technologies*, Novi Sad, Serbia.

Young, B and Hancock, GJ. 2003. Cold-formed steel channels subjected to concentrated bearing load. *Journal of Structural Engineering*, 129(8): 1003-1010.

Zhao, XL and Hancock, GJ. 1992. Square and Rectangular Hollow Sections Subject to Combined Actions. *Journal of Structural Engineering*, 118(3): 648-667.

Zhao, XL and Hancock, GJ. 1995. Square and rectangular hollow sections under transverse end-bearing force. *Journal of Structural Engineering*, 121(9): 1323-1329.

Zhou, F and Young, B. 2007. Experimental and numerical investigations of cold-formed stainless steel tubular sections subjected to concentrated bearing load. *Journal of Constructional Steel Research*, 63(11): 1452-1466.

Zhou, F and Young, B. 2008. Aluminum tubular sections subjected to web crippling-Part I: Tests and finite element analysis. *Thin-Walled Structures*, 46(4): 339-351.